Available online at www.sciencedirect.com
SCIENCE DIRECT®
Journal of Chromatography A, 1097 (2005) 84–97
JOURNAL OF CHROMATOGRAPHY A
www.elsevier.com/locate/chroma

Thermodynamic functions and intraparticle mass transfer kinetics of structural analogues of a template on molecularly imprinted polymers in liquid chromatography

Hyunjung Kim[a,b], Georges Guiochon[a,b,*]

[a] *Department of Chemistry, University of Tennessee, Knoxville, TN 37996-1600, USA*
[b] *Division of Chemical Sciences, Oak Ridge National Laboratory, Oak Ridge, TN 37831-6120, USA*

Received 8 June 2005; received in revised form 3 August 2005; accepted 5 August 2005
Available online 25 August 2005

Abstract

The parameters of the thermodynamics and mass transfer kinetics of the structural analogues (L-enantiomers) of the template were measured on an Fmoc-L-tryptophan (Fmoc-L-Trp) imprinted polymer, at different temperatures. The equilibrium isotherm data and the overloaded band profiles of these compounds were measured at temperatures of 298, 313, 323, and 333 K. The isotherm data were modeled. The thermodynamic functions of the different adsorption sites were derived from the isotherm parameters, using van't Hoff plots. The mass transfer parameters were derived by comparing the experimental peak profiles and profiles calculated using the lumped pore diffusion (POR) model for chromatography. These data show that (1) the strength between the substrate molecules and the MIP increases with increasing number of functional groups on the substrates; (2) enthalpy is the driving force for the affinity of the substrates for the MIP; (3) surface diffusion is the dominant mass transfer mechanism of the substrates through the porous MIP. For those substrate molecules that have the same stereochemistry as the template, the energetic surface heterogeneity needs to be incorporated into the surface diffusion coefficients. Heterogeneous surface diffusivities decrease with increasing affinity of the substrates for the MIP.

Keywords: Fmoc-L-tryptophan imprinted polymers; Frontal analysis; Isotherm parameters; van't Hoff plot; Entropy; Enthalpy; POR model; Surface diffusion; Isosteric heat of adsorption

1. Introduction

Molecularly imprinted polymers (MIPs) are artificial solid adsorbents which provide unprecedented high selectivity for a target molecule that is present in solution during polymerization of the MIP [1]. The strategy most common in the preparation of MIPs consists in using non-covalent interactions between the target molecule (the template) and some suitable functional groups. These interactions allow the formation of template-functional monomer complexes in solution. These complexes are then immobilized into a polymer matrix by copolymerization with a high concentration of cross-linking monomers. Complementary size, shape, and functionalities toward the template in the MIPs can be obtained by extracting the template from the polymer matrix after the polymerization process. Due to their high selectivity, along with their chemical and physical stabilities, MIPs have become popular solid adsorbents for the separation of structurally related substrates or enantiomers. To prepare rationally a MIP for a specific application, we need to understand the thermodynamic driving force and the mass transfer kinetics of the substrate in the binding event with the MIPs.

In previous studies [2,3], we reported equilibrium and mass transfer data for the adsorption of the enantiomers of structural analogues of a template on a Fmoc-L-Trp MIP and on its corresponding non-imprinted polymer (NIP) at room temperature. These analogues were Fmoc-L-tyrosine (Fmoc-L-Tyr), Fmoc-L-serine (Fmoc-L-Ser), Fmoc-L-phenyalanine (Fmoc-L-Phe), Fmoc-L-tryptophan pentafluorophenyl ester (Fmoc-L-Trp(OPfp)), Fmoc-Glycine (Fmoc-Gly), and the antipodes of the first four compounds. This study showed

* Corresponding author. Tel.: +1 865 974 0733; fax: +1 865 974 2667.
E-mail address: guiochon@utk.edu (G. guiochon).

0021-9673/$ – see front matter © 2005 Elsevier B.V. All rights reserved.
doi:10.1016/j.chroma.2005.08.020

a considerable cross-reactivity of the structural analogues, especially those that have the same stereochemistry as the template. The isotherm parameters estimated from the equilibrium isotherm data show that the cross-reactivity of the analogs that have the same stereochemistry as the template increases with increasing number of functional groups of these substrate molecules, while the cross-reactivity of their enantiomers increases with increasing hydrophobicity of these substrates as indicated by their octanol–water partition coefficients. We also found that the mass transfer kinetics of the D-enantiomers on the MIP and of both enantiomers on the NIP are dominantly controlled by surface diffusion. The surface diffusivities decrease with increasing affinity of the substrates for the polymers. However, the surface diffusivities of the substrates on the MIP that have the same stereochemistry as the template (the L-enantiomers) increase with increasing concentration, indicating that the surface heterogeneity needs to be incorporated into the surface diffusion coefficients.

To better understand the thermodynamic and the mass transfer behaviors of the L-enantiomers on the MIP, we acquired the equilibrium isotherm data and the band profiles for the L-enantiomers on the MIP at temperatures of 298, 313, 323, and 333 K. The isotherm data were modeled and the best parameters of the model derived by non-linear regression of the data. The dependency of the isotherm parameters on the temperature afforded the thermodynamic functions of the L-enantiomers on the MIP. Similarly, the dependency of the band profiles on the temperature lead to the temperature dependency of surface diffusion. From this information, we derive a better understanding of the mass transfer kinetic properties of the L-enantiomers on the MIP.

2. Theory

The detailed theoretical background of our approach to modeling the thermodynamics and the intraparticle mass transfer kinetics of molecularly imprinted polymers in liquid chromatography can be found in previous studies [4,5]. We summarize the background material needed to understand the results of this investigation.

2.1. Isotherm models

The isotherm model that was found best to model the isotherm behavior of all the systems studied here is the tri-Langmuir isotherm:

$$q = \frac{q_{s1} b_1 C}{1 + b_1 C} + \frac{q_{s2} b_2 C}{1 + b_2 C} + \frac{q_{s3} b_3 C}{1 + b_3 C} \quad (1)$$

where q is the amount adsorbed and C is the concentration of a substrate in the mobile phase in equilibrium with the adsorbent, q_{s1}, q_{s2}, and q_{s3} are the saturation capacities for the first, second, and third types of adsorption sites that coexist on the heterogeneous surface of the MIP or NIP, respectively; and b_1, b_2, and b_3 are the corresponding association constants.

2.2. Modeling of band profiles

The elution band profiles of large samples of the substrates studied were modeled using the lumped pore diffusion model (POR). Detailed theoretical information on this model is available elsewhere [5–8]. The modeling method consists in simulating the dynamics of band migration in the column by calculating the band profiles, using the lumped pore diffusion model (POR) and the best isotherm model derived from the isotherm data (see above). By minimizing the difference between the calculated and the experimental band profiles, we determine the intraparticle diffusion coefficient.

3. Experimental

We summarize the essential experimental conditions relevant to our current study. Other details can be found in previous publications [4,5].

3.1. Preparation of the stationary phase and packing of the column

The MIP was prepared by thermal polymerization, using 4-vinylpyridine (4-VPY) and ethylene glycol dimethacrylate (EGDMA) as the functional monomer and the cross-linking monomer, respectively. The components of the polymerization mixtures were: 1.58 mmol Fmoc-L-Trp, 4.74 mmol 4-VPY, 18.96 mmol EGDMA, 0.474 mmol AIBN, and 5.4 ml acetonitrile (MeCN). The amount of solvent was 4/3 of the total volume of the monomers and the cross-linking monomers. The solution was purged with N_2 for 5 min in a scintillation vial and polymerized at 45 °C for 12 h. After polymerization, the bulk polymers were crushed, ground, and sieved to obtain particles within the size range of 25–38 mm. The resulting particles were packed into a stainless steel column (10 cm × 0.48 cm). The mobile phase was acetonitrile with one percent of acetic acid as the organic modifier. The total porosity of the MIP column was 0.737 and its external porosity 0.368. Details on the synthesis of the polymers and the measurements of the column parameters are provided elsewhere [4,5].

3.2. Procedures

Frontal analysis was used to acquire the isotherm data of each substrate on the MIP at temperatures of 298, 313, 323, and 333 K. The substrate concentrations ranged between 0.005 and 40 mM. Each breakthrough curve was acquired by flushing the column with a stream of known concentration of a substrate until the concentration of the effluent is the same as that of the influx for at least 5 min, indicating equilibrium of the substrate in the column. Thirty successive breakthrough curves were obtained at increasing concentrations, the column being flushed with the pure mobile phase between successive breakthrough curves. Each breakthrough curve provides one isotherm data point, the amount of the

Table 1
The tri-Langmuir isotherm parameters of the equilibrium isotherm data for L-enantiomers on the Fmoc-L-Trp MIP

Substrate	T (K)	F_{cal}	q_1 (mM)	b_1(mM^{-1})	q_1b_1	q_2 (mM)	b_2 (mM^{-1})	q_2b_2	q_3 (mM)	b_3 (mM^{-1})	q_3b_3	$(qb)_t$
L-Trp	298	1360	482 ± 14	0.0342 ± 0.02	16.5 ± 1.1	19.2 ± 1.8	0.968 ± 0.084	18.6 ± 2.4	0.599 ± 0.030	99.6 ± 8.1	59.7 ± 5.7	94.7 ± 6.3
	313		482 ± 14	0.02003 ± 0.0011	9.65 ± 0.60	19.2 ± 1.8	0.634 ± 0.057	12.2 ± 1.6	0.599 ± 0.030	54.7 ± 3.9	32.8 ± 2.9	54.6 ± 3.3
	323		482 ± 14	0.0182 ± 0.00096	8.77 ± 0.53	19.2 ± 1.8	0.451 ± 0.040	8.66 ± 1.1	0.599 ± 0.030	41.4 ± 2.4	24.8 ± 1.9	42.2 ± 2.3
	333		482 ± 14	0.0151 ± 0.00079	7.28 ± 0.44	19.2 ± 1.8	0.371 ± 0.033	7.12 ± 0.92	0.599 ± 0.030	36.5 ± 2.2	21.9 ± 1.7	36.3 ± 2.0
L-Tyr	298	2046	488 ± 11	0.0432 ± 0.0023	21.1 ± 1.2	19.7 ± 1.9	1.44 ± 0.14	28.4 ± 3.9	0.293 ± 0.023	160 ± 15	46.9 ± 5.7	96.3 ± 7.03
	313		488 ± 11	0.0288 ± 0.0015	14.05 ± 0.80	19.7 ± 1.9	0.9081 ± 0.086	17.9 ± 2.4	0.293 ± 0.023	62.8 ± 5.4	18.4 ± 2.1	50.34 ± 3.3
	323		488 ± 11	0.024 ± 0.0012	11.7 ± 0.64	19.7 ± 1.9	0.6904 ± 0.067	13.6 ± 1.9	0.293 ± 0.023	76.1 ± 6.8	22.3 ± 2.7	47.6 ± 3.3
	333		488 ± 11	0.0194 ± 0.00098	9.47 ± 0.52	19.7 ± 1.9	0.538 ± 0.052	10.60 ± 1.4	0.293 ± 0.023	61.5 ± 5.4	18.02 ± 2.1	38.09 ± 2.6
L-Ser	298	491	650.3 ± 17	0.0228 ± 0.0011	14.8 ± 0.81	20.13 ± 1.7	0.782 ± 0.061	15.7 ± 1.8	0.189 ± 0.018	90.3 ± 12	17.07 ± 2.8	47.6 ± 3.4
	313		650.3 ± 17	0.0159 ± 0.00077	10.34 ± 0.57	20.13 ± 1.7	0.529 ± 0.041	10.65 ± 1.2	0.189 ± 0.018	53.3 ± 6.2	10.07 ± 1.5	31.06 ± 2.02
	323		650.3 ± 17	0.0131 ± 0.00063	8.51 ± 0.47	20.13 ± 1.7	0.4201 ± 0.033	8.46 ± 0.98	0.189 ± 0.018	44.8 ± 5.3	8.47 ± 1.3	25.4 ± 1.7
	333		650.3 ± 17	0.01068 ± 0.00051	6.95 ± 0.38	20.13 ± 1.7	0.344 ± 0.027	6.92 ± 0.80	0.189 ± 0.018	34.3 ± 3.7	6.48 ± 0.93	20.35 ± 1.3
L-Phe	298	2470	336 ± 11	0.05103 ± 0.0027	17.1 ± 1.1	3.63 ± 0.49	3.16 ± 0.46	11.5 ± 2.3	0.0887 ± 0.0099	156 ± 22	13.8 ± 2.5	42.5 ± 3.5
	313		336 ± 11	0.035 ± 0.0018	11.8 ± 0.72	3.63 ± 0.49	2.24 ± 0.33	8.13 ± 1.6	0.0887 ± 0.0099	138 ± 17	12.2 ± 2.03	32.1 ± 2.7
	323		336 ± 11	0.0285 ± 0.0014	9.58 ± 0.56	3.63 ± 0.49	1.67 ± 0.24	6.062 ± 1.2	0.0887 ± 0.0099	121 ± 15	10.73 ± 1.8	26.4 ± 2.2
	333		336 ± 11	0.0228 ± 0.0011	7.66 ± 0.45	3.63 ± 0.49	1.13 ± 0.17	4.102 ± 0.83	0.0887 ± 0.0099	100.9 ± 13	8.95 ± 1.5	20.71 ± 1.8

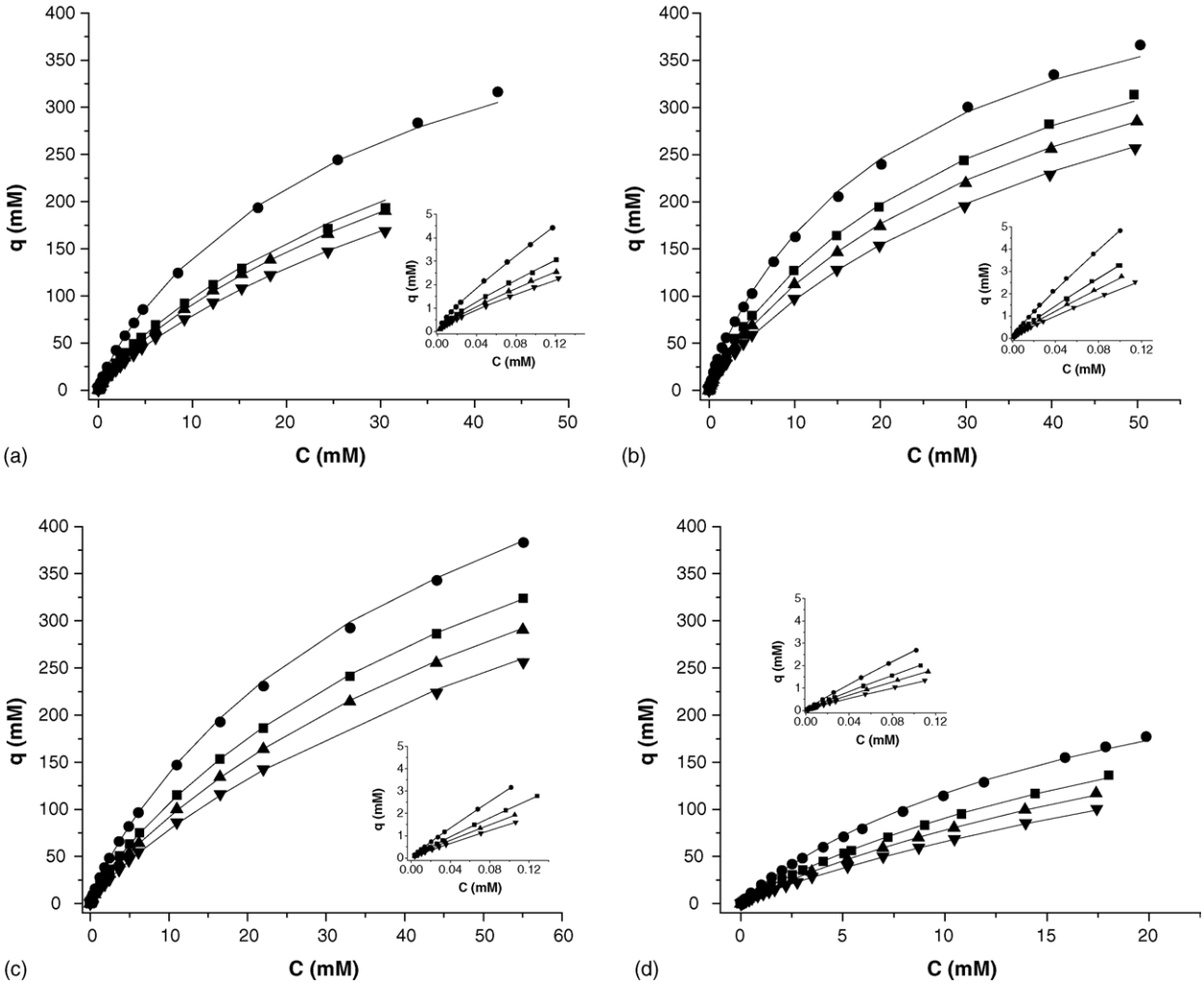

Fig. 1. Adsorption equilibrium isotherms on an Fmoc-L-Trp MIP at temperatures of 298 K (circles), 313 K (squares), 323 K (triangle-ups), and 333 K (triangle-downs) of: (a) Fmoc-L-Trp; (b) Fmoc-L-Tyr; (c) Fmoc-L-Ser; (d) Fmoc-L-Phe. The symbols represent the experimental data and the solid lines represent the best tri-Langmuir isotherms. The inset in each figure shows the adsorption isotherms at lowest concentration ranges between 0.005 and 0.12 mM.

substrate adsorbed (q, mM) versus the substrate concentration in the mobile phase (C, mM). The amounts q adsorbed were calculated from the retention time of the breakthrough curve, using the equal area method [9]. The experimental isotherm data were fitted to isotherm models and the quality of the fits were compared using the standard deviations of all the isotherm parameters, the Fisher parameter, and the residual sum of squares.

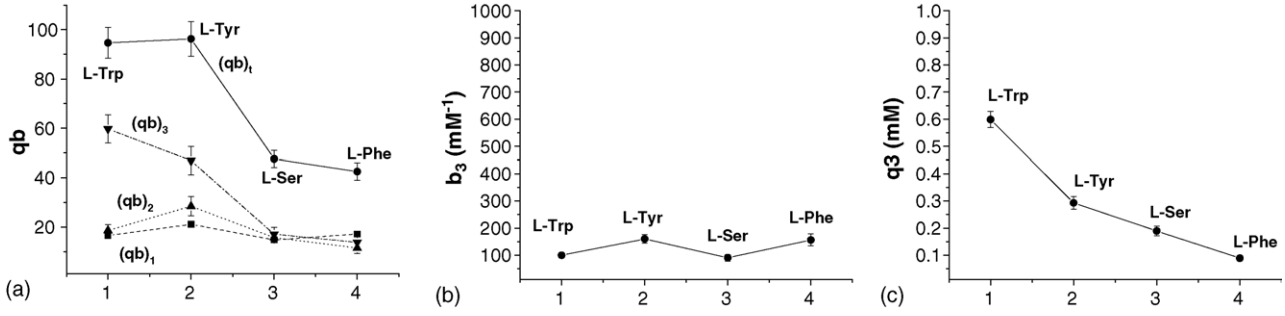

Fig. 2. Characteristics of the equilibrium isotherms. Plots of: (a) affinity (i.e., the product of q *and* b) of each substrate on each identified site and the overall affinity; (b) association constant of each substrate on the highest energy site (site 3); (c) saturation capacity of each substrate on the highest energy site (site 3). For clarity, x-axis was randomly chosen in such a way that the decreasing trends were observed.

Experimental band profiles of large samples of the L-enantiomers on the MIP were recorded at each temperature when the frontal analysis data were acquired. Six solutions of concentrations ranging between 0.1 and 40 mM were injected for 1 min with the pump running at 1 mL/min (i.e., sample sizes were between 0.1 and 40 μmol). The band profiles, like the breakthrough curves, were recorded at wavelengths of 260 and 310 nm, depending on the concentration, and the absorbance data (mAU) were converted into concentrations (mM) by estimating the numerical coefficients of a second order polynomial [5].

4. Results and discussion

The thermodynamic and the mass transfer kinetics of structural analogues of the template on the MIP were studied by acquiring and modeling the FA adsorption isotherm data and high-concentration band profiles. The structural analogues studied have the same stereochemistry as the template (L-enantiomers). The structural analogues of the template studied have a different number of functional groups that can interact with the functional 4-vinylpyridine groups on the polymer surface. There are two such functional groups in Fmoc-L-tyrosine (Fmoc-L-Tyr) and Fmoc-L-serine (Fmoc-L-Ser) and one group in Fmoc-L-tryptophan (Fmoc-L-Trp) and Fmoc-L-phenylalanine (Fmoc-L-Phe). The strength of the hydrophobicity of the substrates, estimated from the octanol–water partition coefficient (log P_{ow}) [10], decreases in the following order: (1) for the substrates with two OH functional groups, Fmoc-L-Tyr (log $P_{ow} = 4.17$)>Fmoc-L-Ser (log $P_{ow} = 1.48$); (2) for the substrates with one OH functional group, Fmoc-L-Trp (log $P_{ow} = 4.74$)> Fmoc-L-Phe (log $P_{ow} = 4.65$).

4.1. Studies of thermodynamic parameters

Fig. 1 shows the FA adsorption isotherm data obtained for Fmoc-L-Trp (Fig. 1(a)), for Fmoc-L-Tyr (Fig. 1(b)), for Fmoc-L-Ser (Fig. 1(c)), and for Fmoc-L-Phe (Fig. 1(d)) on the Fmoc-L-Trp imprinted polymer at the temperatures of 298 K (circles), 313 K (squares), 323 K (triangle-ups), and 333 K (triangle-downs). An inset in each figure shows the low concentration data (0.005–0.10 mM). A rapid survey shows that all these isotherms are langmuirian. At any given mobile phase concentration, the amount adsorbed at equilibrium decreases always with increasing temperature. At a given temperature, the amount adsorbed decreases in the following order:

$$\text{Fmoc-L-Trp} \simeq \text{Fmoc-L-Tyr} > \text{Fmoc-L-Ser} > \text{Fmoc-L-Phe}.$$

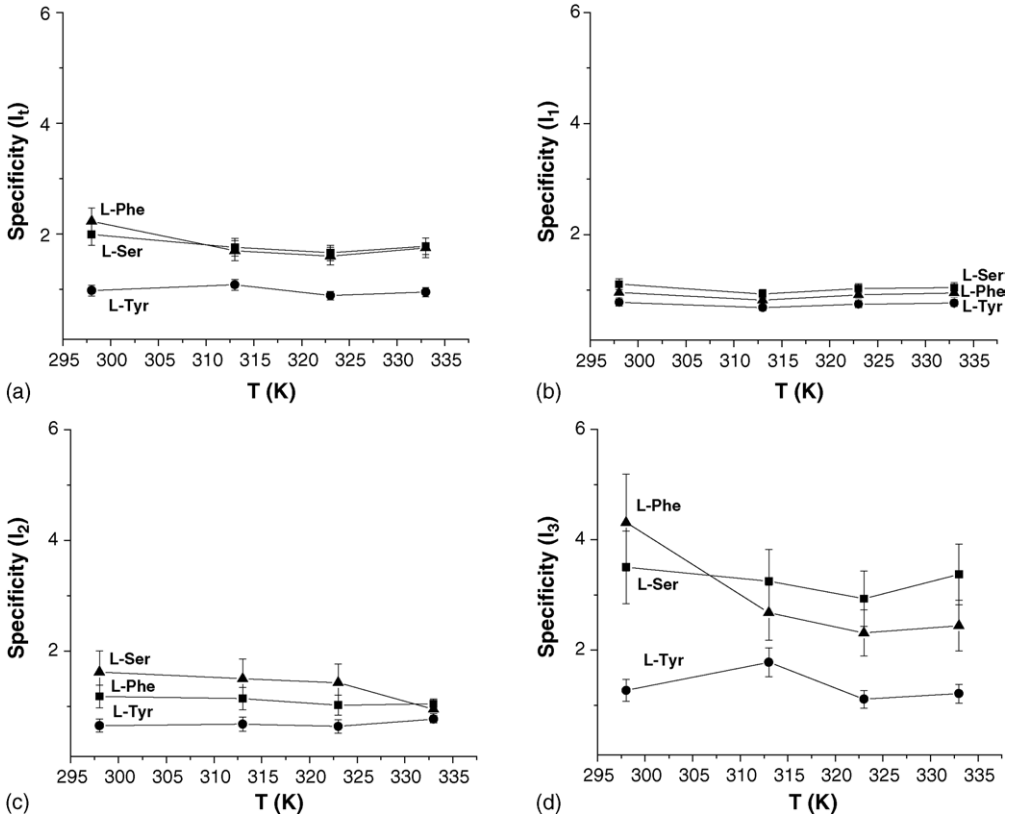

Fig. 3. Plots vs. the temperature of the selectivity toward the template (Fmoc-L-Trp) against the other structural analogues (i.e., of the the affinity toward Fmoc-L-Trp divided by that toward the other substrates) on: (a) the entire surface of the MIP; (b) the site 1; (c) the site 2; (d) the site 3. The sites of types 1–3 correspond to the energy modes identified from the non-linear regression (see Table 1).

This trend indicates that increasing the number of functional groups on a substrate seems to increase the interactions between the substrate and the MIP. The solid lines in Fig. 1 represent the best isotherm model for the isotherm data, which in all cases is the tri-Langmuir isotherm model. This result is in agreement with those of previous reports [11,12] which showed that a multi-Langmuir isotherm model accounts well for the isotherm data of substrates on MIPs, better than other continuous isotherm models such as the Freundlich or the Langmuir-Freundlich isotherm models. Using the multi-Langmuir isotherm model for enantiomers on the MIPs provides the important advantage of permitting the separation of the selective and the nonselective interactions within the investigated concentration range. The best tri-Langmuir isotherm parameters for the different systems studied are summarized in Table 1.

The isotherm parameters afford the overall affinity and the affinity of each substrate for each identified type of sites. These affinities are the products $b_i q_{s,i}$ of the association constant and the saturation capacity for the sites of type i, the overall affinity being the sum $\sum_1^3 b_i q_{s,i}$. Fig. 2(a) shows that the overall affinity of each substrate on the MIP at 298 K decreases in the following order:

$$\text{Fmoc-L-Trp} \simeq \text{Fmoc-L-Tyr} > \text{Fmoc-L-Ser} > \text{Fmoc-L-Phe}$$

Note that the x-axis in this figure is arbitrary. Fig. 2(a) shows also that the contribution of the affinity of the substrate for the highest energy sites dominates the overall affinity of the first two substrates, Fmoc-L-Tyr and the template. The substrates have markedly different affinities for the highest energy type of sites. This is due to the large variations of the density of these sites (Fig. 2(c)) while the association constant remains almost constant (Fig. 2(a)). The selectivity of the MIP against a substrate is the ratio of the affinity of the template to that of the substrate. From the isotherm parameters of the substrates at each temperature, we derive these specificities (Fig. 3) on each identified type of sites of the MIP. Fig. 3 shows that the selectivity against a substrate on the highest energy type of sites (Fig. 3(d)) gives the dominant contribution to the overall selectivity (Fig. 3(a)). The selectivity against the substrates on the highest energy type of sites at room temperature (298 K) decreases in the following order:

$$\text{Fmoc-L-Phe} > \text{Fmoc-L-Ser} > \text{Fmoc-L-Tyr}$$

Increasing the temperature provided no significant change in the relative selectivity of the MIP toward the template or toward Fmoc-L-Phe or Fmoc-L-Ser. Fig. 3 also shows that

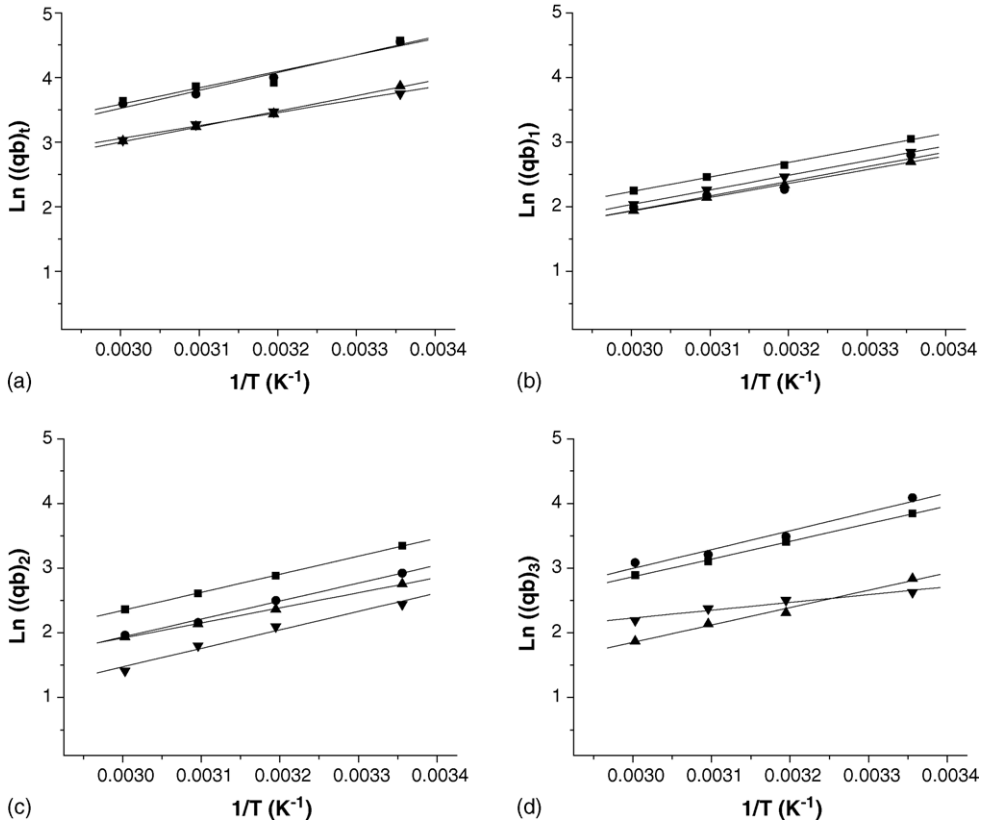

Fig. 4. van't Hoff plot for the determination of the enthalpy of adsorption of Fmoc-L-Trp (closed circles), Fmoc-L-Tyr (closed squares), Fmoc-L-Ser (closed triangle-ups), and Fmoc-L-Phe (closed triangle-downs) on: (a) the overall sites; (b) the site 1; (c) the site 2; (d) the site 3. The symbols represent the experimental data; the lines represent the best linear fits. The indices site 1, site 2, and site 3 correspond to the types of sites identified on the polymer surface.

there is no significant selectivity against Fmoc-L-Tyr, within the experimental errors. There is no significant change of the selectivity against a substrate with increasing temperature while the affinity of each substrate decreases markedly. For example, increasing the temperature from 298 to 333 K causes a slight decrease of the selectivity against Fmoc-L-Tyr (3.9%) on the highest energy type of sites. On the other hand, the affinity for Fmoc-L-Tyr decreases by 62% on these sites if the temperature increases from 298 to 333 K. Similar results were observed previously for the separation of the Fmoc-Trp enantiomers on the Fmoc-L-Trp MIP [13]. In summary, comparing the isotherm parameters of the structural analogues on the MIP shows that the contributions of the highest energy type of sites to the affinity of the different substrates and to the selectivity against them seem to be controlled by the number of functional groups on the substrate that can interact with the MIP. The selectivity against a substrate is highest on the highest energy type of sites and does not vary significantly with increasing temperature.

Better to understand the driving force for the affinity of the different substrates for the MIP, we calculated the thermodynamic functions of adsorption by applying the van't Hoff equation (Eq. (2)) [14–17] to each identified type of sites on the MIP.

$$\frac{\partial(\ln(q_s b)_i)}{\partial(1/T)} = \frac{-\Delta H_i^\circ}{R} \quad (2)$$

where $q_{s,i}$ and b_i are the saturation capacities and the association constant associated with each type of sites (see Table 1) and ΔH_i° is the corresponding standard molar enthalpy of adsorption. Fig. 4 shows a plot of the logarithm of the coefficients $b_i q_{s,i}$ versus the reciprocal of the temperature for Fmoc-L-Trp (closed circles), Fmoc-L-Tyr (closed squares), Fmoc-L-Ser (closed triangle-ups), and Fmoc-L-Phe (closed triangle-downs) on the overall sites (Fig. 4(a)), on the sites of

Table 2
Thermodynamic functions for L-enantiomers on the MIP derived from isotherm data using van't Hoff equation

Site	Thermodynamic parameters	T (K)	L-Trp	L-Tyr	L-Ser	L-Phe
1	ΔG (kcal/mol)	298	−1.66	−1.805	−1.60	−1.68
		313	−1.41	−1.64	−1.45	−1.53
		323	−1.39	−1.58	−1.38	−1.45
		333	−1.31	−1.49	−1.28	−1.35
	ΔH (kcal/mol)	298	−4.57	−4.57	−4.25	−4.51
		313	−4.57	−4.57	−4.25	−4.51
		323	−4.57	−4.57	−4.25	−4.51
		333	−4.57	−4.57	−4.25	−4.51
	ΔS (cal/mol/K)	298	−9.77	−9.28	−8.91	−9.49
		313	−10.10	−9.35	−8.94	−9.51
		323	−9.83	−9.26	−8.91	−9.48
		333	−9.78	−9.26	−8.92	−9.50
2	ΔG (kcal/mol)	298	−1.73	−1.98	−1.63	−1.44
		313	−1.55	−1.79	−1.47	−1.304
		323	−1.39	−1.68	−1.37	−1.16
		333	−1.30	−1.56	−1.28	−0.934
	ΔH (kcal/mol)	298	−5.56	−5.56	−4.65	−5.76
		313	−5.56	−5.56	−4.65	−5.76
		323	−5.56	−5.56	−4.65	−5.76
		333	−5.56	−5.56	−4.65	−5.76
	ΔS (cal/mol/K)	298	−12.9	−12.02	−10.1	−14.5
		313	−12.8	−12.05	−10.2	−14.2
		323	−12.9	−12.04	−10.2	−14.3
		333	−12.8	−12.02	−10.1	−14.5
3	ΔG (kcal/mol)	298	−2.42	−2.28	−1.68	−1.56
		313	−2.17	−1.81	−1.44	−1.56
		323	−2.061	−1.99	−1.37	−1.52
		333	−2.041	−1.91	−1.24	−1.45
	ΔH (kcal/mol)	298	−5.76	−5.37	−5.37	−2.38
		313	−5.76	−5.37	−5.37	−2.38
		323	−5.76	−5.37	−5.37	−2.38
		333	−5.76	−5.37	−5.37	−2.38
	ΔS (cal/mol/K)	298	−11.2	−10.4	−12.4	−2.78
		313	−11.5	−11.4	−12.6	−2.64
		323	−11.5	−10.4	−12.4	−2.66
		333	−11.2	−10.4	−12.4	−2.81

Table 3
Thermodynamic functions for the specificity toward the template (Fmoc-L-Trp) vs. the other L-enantiomers on the MIP derived from isotherm data using van't Hoff equation

T (K)	L-Tyr			L-Ser			L-Phe		
	Site 1	Site 2	Site 3	Site 1	Site 2	Site 3	Site 1	Site 2	Site 3
$\Delta\Delta G$ (kcal/mol)									
298	0.145	0.25	−0.14	−0.06	−0.1	−0.74	0.02	−0.29	−0.86
313	0.23	0.24	−0.36	0.04	−0.08	−0.73	0.12	−0.246	−0.61
323	0.19	0.29	−0.071	−0.01	−0.02	−0.691	0.06	−0.23	−0.541
333	0.18	0.26	−0.131	−0.03	−0.02	−0.801	0.04	−0.366	−0.591
$\Delta\Delta H$ (kcal/mol)									
298	0	0	−0.39	−0.32	−0.91	−0.39	−0.06	0.2	−3.38
313	0	0	−0.39	−0.32	−0.91	−0.39	−0.06	0.2	−3.38
323	0	0	−0.39	−0.32	−0.91	−0.39	−0.06	0.2	−3.38
333	0	0	−0.39	−0.32	−0.91	−0.39	−0.06	0.2	−3.38
$\Delta\Delta G$ (kcal/mol)									
298	−0.49	−0.88	−0.8	−0.86	−2.8	1.2	−0.28	1.6	−8.42
313	−0.75	−0.75	−0.1	−1.16	−2.6	1.1	−0.59	1.4	−8.86
323	−0.57	−0.86	−1.1	−0.92	−2.7	0.9	−0.35	1.4	−8.84
333	−0.52	−0.78	−0.8	−0.86	−2.7	0.2	−0.28	1.7	−8.39

type 1 (Fig. 4(b)), type 2 (Fig. 4(c)), and type 3 (Fig. 4(d)). The solid lines are the best linear fit of the data to the van't Hoff equation. The standard molar enthalpy of adsorption, ΔH_i°, was derived from the slope of these lines, and the standard molar Gibbs free energy of the corresponding site, ΔG_i°, was derived from the following Eq. (3):

$$\Delta G_i^\circ = -RT \ln K_i = -RT \ln(q_s b)_i \quad (3)$$

where R is the universal gas constant (1.9872 cal/mol/K) and $K_i = q_{s,i} b_i$. From these two values, the standard molar entropy of adsorption, ΔS°, for the corresponding site can be estimated from Eq. (4):

$$\Delta S_i^\circ = -\frac{(\Delta G_i^\circ - \Delta H_i^\circ)}{T} \quad (4)$$

These values are reported in Table 2. Negative values of ΔG_i°, ΔH_i°, and ΔS_i° were observed at all temperatures and at each idetified site. These negative values of the thermodynamic functions for the different substrates show that the transfer of the substrates from the mobile phase to the stationary phase is enthalpically favorable. The absolute values of ΔH_i° are between 10 and 20 kJ/mol (i.e., between 2 and 5 kcal/mol) on the highest energy type of sites (type 3).

Table 4
Values of parameters for L-enantiomers on the MIP[a] used in the POR model

Substrate	Temperature (K)	η (cp)[b]	d(g/cm^3)	D_m[c] $\times 10^{-3}$ (cm^2/min)	k_{ext}[d] (cm/min)	D_L[e] (cm^2/min)
L-Trp	298	0.348	0.777	0.627	1.88	0.052
	313	0.3068	0.7606	0.746	2.11	0.0463
	323	0.283	0.750	0.835	2.27	0.0428
	333	0.262	0.738	0.931	2.44	0.0395
L-Tyr	298	0.348	0.777	0.648	1.84	0.0531
	313	0.3068	0.7606	0.771	2.059	0.0474
	323	0.283	0.750	0.862	2.22	0.0438
	333	0.262	0.738	0.962	2.39	0.0405
L-Ser	298	0.348	0.777	0.725	2.023	0.0483
	313	0.3068	0.7606	0.863	2.27	0.0427
	323	0.283	0.750	0.965	2.45	0.0393
	333	0.262	0.738	1.077	2.63	0.0363
L-Phe	298	0.348	0.777	0.669	1.91	0.0511
	313	0.3068	0.7606	0.796	2.16	0.0452
	323	0.283	0.750	0.891	2.32	0.0418
	333	0.262	0.738	0.994	2.50	0.0385

[a] ϵ_t total porosity = 0.737, ϵ_e external porosity = 0.368, ϵ_p internal porosity = $(\epsilon_t - \epsilon_e)/(1 - \epsilon_e) = 0.584$, tortuosity = $(2 - \epsilon_p)^2/\epsilon_p = 3.43$.
[b] Viscosity and density of the mobile phase (acetonitrile) were taken from Perry's Chemical Handbook.
[c] Molecular diffusion coefficient of the solute in the mobile phase (see Eq. (10) in Section 2).
[d] External mass transfer coefficient.
[e] Dispersion coefficient.

Table 5
Heterogeneous surface diffusivities ($D_s(Q_{st})$) derived from Eq. (11)

T (K)	$D_s(Q_{st})$ ($\times 10^{-6}$) (cm^2/min)				
	q	L-Trp	L-Tyr	L-Ser	L-Phe
298	0.1	0.456	0.7059	1.11	1.14
	0.5	0.564	0.700	1.27	1.66
	1	0.641	0.695	1.36	1.19
	5	0.786	0.717	1.43	1.39
	10	0.899	0.795	1.47	1.56
	50	1.55	1.29	1.63	1.79
	100	1.80	1.48	1.68	1.81
313	0.1	–	1.21	2.55	1.94
	0.5	–	1.21	2.82	1.97
	1	–	1.20	2.96	2.02
	5	–	1.22	3.08	2.31
	10	–	1.29	3.15	2.55
	50	–	1.69	3.41	2.88
	100	–	1.82	3.48	2.90
323	0.1	1.108	1.36	2.21	2.52
	0.5	1.340	1.36	2.48	2.58
	1	1.504	1.35	2.62	2.64
	5	1.805	1.38	2.74	3.06
	10	2.037	1.46	2.81	3.41
	50	3.31	1.94	3.09	3.9
	100	3.804	2.10	3.16	3.92
333	0.1	1.67	1.89	2.74	3.26
	0.5	1.97	1.88	3.06	3.33
	1	2.18	1.88	3.22	3.40
	5	2.55	1.91	3.37	3.9
	10	2.83	2.02	3.45	4.31
	50	4.33	2.63	3.76	4.88
	100	4.88	2.83	3.85	4.90

The thermodynamic functions for the selectivity against the different structural analogues (i.e., $\Delta(\Delta H^\circ)$, $\Delta(\Delta S^\circ)$, and $\Delta(\Delta G^\circ)$) were obtained as follows:

$$\begin{aligned}\Delta(\Delta H^\circ) &= \Delta H^\circ\,(\text{Fmoc-L-Trp}) - \Delta H^\circ\,(\text{substrate})\\ \Delta(\Delta S^\circ) &= \Delta S^\circ\,(\text{Fmoc-L-Trp}) - \Delta S^\circ\,(\text{substrate})\\ \Delta(\Delta G^\circ) &= \Delta G^\circ\,(\text{Fmoc-L-Trp}) - \Delta G^\circ\,(\text{substrate})\end{aligned} \quad (5)$$

These values are reported in Table 3. On the highest energy type of sites (type 3), the values of $\Delta(\Delta G^\circ)$, $\Delta(\Delta H^\circ)$, and $\Delta(\Delta S^\circ)$ are negative at all temperatures, showing that the favorable free energy of adsorption of the template (Fmoc-L-

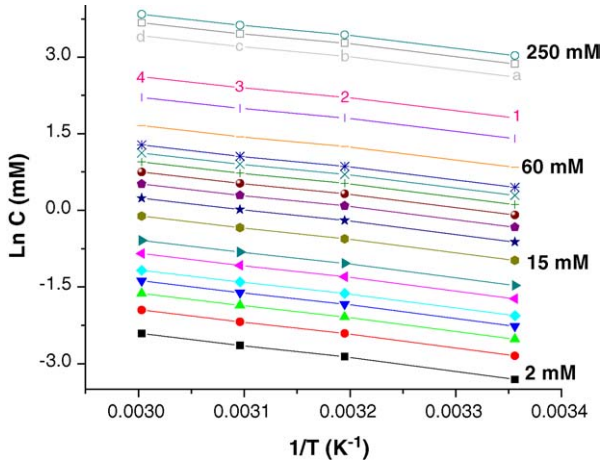

Fig. 5. Representative plot between $\ln(C)$ and $1/T$ for determining Q_{st} for Fmoc-L-Tyr on the MIP.

Table 6
Values of parameters p_1, p_2, p_3, p_4 and p_5 in Eq. (10) for L-enantiomers on the MIP

Substrate	p_1 (K^{-1})	p_2 (K^{-1})	p_3 (mM^{-1})	p_4 (K^{-1})	p_5 (mM^{-1})
Fmoc-L-Trp	2103 ± 0.57	153 ± 15	1.79 ± 0.15	338 ± 0.92	0.0339 ± 0.00025
Fmoc-L-Tyr	2230 ± 0.57	−54.4 ± 7.6	0.379 ± 0.084	316 ± 3.4	0.0349 ± 0.00049
Fmoc-L-Ser	2130 ± 0.27	128 ± 1.8	2.31 ± 0.047	93.09 ± 0.49	0.0322 ± 0.00048
Fmoc-L-Phe	2270 ± 14	24.3 ± 6.3	0.0166 ± 0.026	291 ± 12	0.137 ± 0.0064

Table 7
Values for parameters in Eq. (11) for L-enantiomers on the MIP

Substrates	T (K)	$-\alpha$	D_{so} (cm^2/min)
L-Trp	298	0.9032 ± 0.0024	$0.001094 \pm 1.8 \times 10^{-5}$
	323	0.879 ± 0.0038	$0.00120 \pm 3.8 \times 10^{-5}$
	333	0.791 ± 0.011	$7.42 \times 10^{-4} \pm 5.9 \times 10^{-5}$
L-Tyr	298	0.87 ± 0.0035	$0.001021 \pm 2.5 \times 10^{-5}$
	313	0.5501 ± 0.0056	$6.504 \times 10^{-5} \pm 8.9 \times 10^{-6}$
	323	0.5501 ± 0.025	$9.501 \times 10^{-5} \pm 6.1 \times 10^{-6}$
	333	0.531 ± 0.0048	$1.002 \times 10^{-4} \pm 8.1 \times 10^{-5}$
L-Ser	298	0.636 ± 0.0026	$1.59 \times 10^{-4} \pm 2.5 \times 10^{-6}$
	313	0.5093 ± 0.0024	$1.12 \times 10^{-4} \pm 1.7 \times 10^{-6}$
	323	0.607 ± 0.0065	$1.74 \times 10^{-4} \pm 7.5 \times 10^{-6}$
	333	0.594 ± 0.027	$1.73 \times 10^{-4} \pm 3.1 \times 10^{-5}$
L-Phe	298	0.480 ± 0.0029	$7.058 \times 10^{-5} \pm 1.5 \times 10^{-6}$
	313	0.442 ± 0.0043	$7.206 \times 10^{-5} \pm 2.2 \times 10^{-6}$
	323	0.498 ± 0.0077	$1.309 \times 10^{-4} \pm 7.6 \times 10^{-6}$
	333	0.475 ± 0.0081	$1.26 \times 10^{-4} \pm 7.9 \times 10^{-6}$

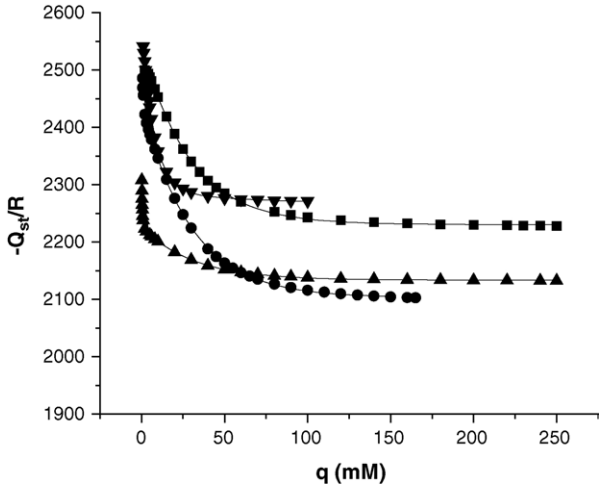

Fig. 6. The dependency of isosteric heat of adsorption, $(-Q_{st}/R)$, on surface concentration (q) for Fmoc-L-Trp (closed circles), Fmoc-L-Tyr (closed squares), Fmoc-L-Ser (closed triangle-ups), and Fmoc-L-Phe (closed triangle-downs). The solid lines represent best fit parameters calculated using Eq. (10).

Trp) versus the other substrates on the MIP is enthalpically driven. These results show that different thermodynamic driving forces are operative in the separation of the structural analogues which have the same stereochemistry as the template and in that of their enantiomers. In a previous study [11], it was found that the separation on a MIP of the enantiomers of the analogues having the structure of the template is entropically driven and their separation increases with increasing hydrophobicity of the substrates. Similar observations were also reported for the enantiomeric separation on a MIP in an aqueous mobile phase [18,19].

4.2. Studies of intraparticle mass transfer kinetics

The experimental band profiles of large samples of the L-enantiomers (sample concentration between 0.1 and 40 mM, volume 1 mL) were acquired on the MIP at each temperature. These peak profiles were compared to those calculated using the lumped pore diffusion model (POR) to estimate the intraparticle diffusion coefficients [5,6]. Table 4 summarizes the values at each temperature of the different parameters necessary to perform these calculations. These parameters are the total column porosity (ε_t), the external column porosity (ε_e), and the internal column porosity (ε_p), the bed tortuosity (γ), the molecular diffusion coefficient in the bulk phase (D_m), and the axial dispersion coefficient (D_L).

In a previous study on the mass transfer kinetics of different substrates on the Fmoc-L-Trp MIP and on the corresponding NIP at room temperature [3], we compared different

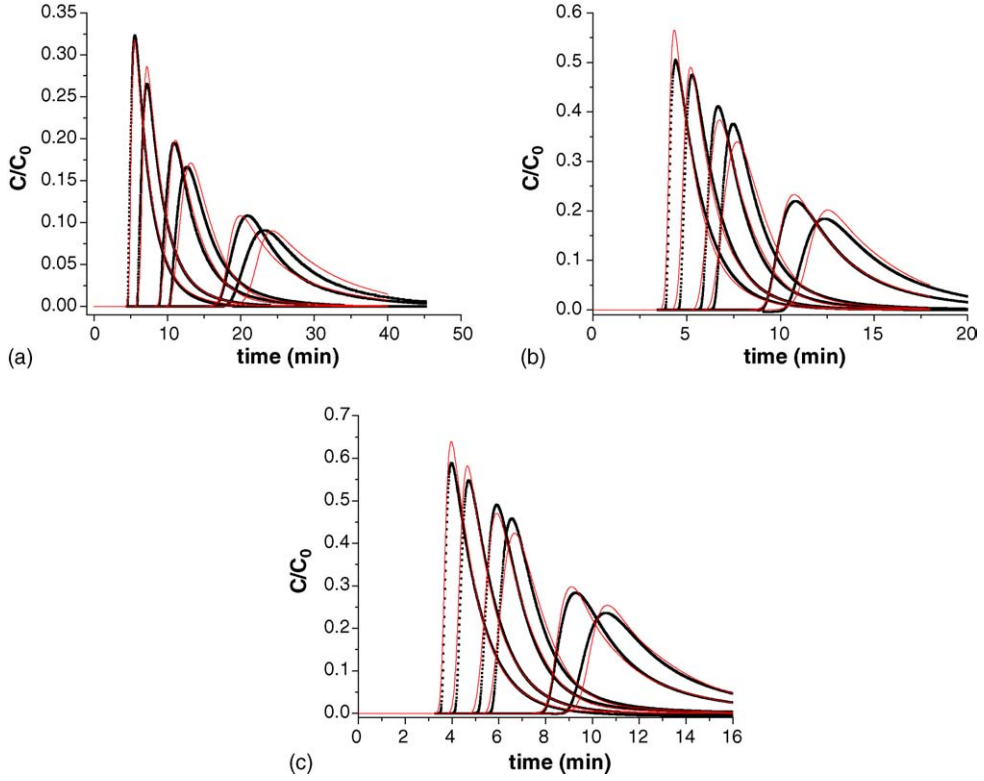

Fig. 7. Comparison between calculated and experimental peak profiles of: (a) Fmoc-L-Trp at 298 K; (b) Fmoc-L-Trp at 323 K; (c) Fmoc-L-Trp at 333 K. The y-axis is normalized by dividing the elute concentration with the injected concentration of the samples. The injection time was equal to 1 min. The following inlet concentrations were used: at 298 K 0.117, 0.234, 2.38, 4.75, 21.2, and 42.5 mM; at 323 K 0.121, 0.238, 2.35, 4.69, 15.2, and 30.50 mM; at 333 K 0.123, 0.246, 2.35, 4.705, 15.3, and 30.503 mM (peaks from right to left). The best values of parameters used to simulate these peak profiles are summarized in Table 7.

intraparticle diffusion models to account for the mass transfer kinetics on the MIP and the NIP. In that study, we showed that the homogeneous surface diffusion model accounts excellently for the mass transfer kinetics of the L-enantiomers on the NIP and for that of the D-enantiomers on the MIP. However, when the substrates have the same stereochemistry as the template (Fmoc-L-Trp), we observed that the apparent surface diffusivities estimated from the homogeneous surface diffusion model increase with increasing concentrations of injected substrates (see Table 5). Similar observation was also made for a L-phenylalanine anilide MIP in an aqueous buffer-organic solvent mixture [20]. This behavior suggests a model error. To account for this dependency of the surface diffusivities of the L-enantiomers on the concentration, we used heterogeneous surface diffusion model [21]. In this model, Arrhenius equation (Eq. (6)) is used to analyze the temperature dependence of surface diffusion (D_S):

$$D_S = D_{S0} \exp\left(\frac{-E_S}{RT}\right) \tag{6}$$

where D_{S0} is the diffusivity at zero energy level, E_S the activation energy of the process, T the temperature in K, and R is the universal gas constant.

The activation energy (E_S) is approximated as a certain fraction of the isosteric heat of adsorption, (Q_{st}), giving the following equation:

$$E_S = \alpha(-Q_{st}) \tag{7}$$

Substitution of Eq. (7) into Eq. (6) gives the surface diffusion coefficient which is a function of the isosteric heat of adsorption:

$$D_S = D_{S0} \exp\left(\frac{-\alpha(-Q_{st})}{RT}\right) = D_{S0} \exp\left(\frac{-\alpha}{T}\left(\frac{-Q_{st}}{R}\right)\right) \tag{8}$$

The isosteric heat of adsorption is determined at constant amount of compound adsorbed (q) by the following equation:

$$\frac{-Q_{st}}{R} = \left[\frac{\mathrm{d}(\ln C)}{\mathrm{d}(1/T)}\right]_{q=\text{constant}} \tag{9}$$

To determine the isosteric heat of adsorption using Eq. (9), we first calculated the value of ln(C) at constant q for each temperature, using the isotherm parameters obtained for each substrate. Fig. 5 shows the plot of ln(C) versus $1/T$ at constant amount adsorbed for Fmoc-L-Tyr as representative compounds. An almost linear relationship between ln(C) and $1/T$ is observed in all cases. The value of Q_{st} was derived from the average slope of these lines. Fig. 6 shows the exponential relationship between the isosteric heat of adsorption

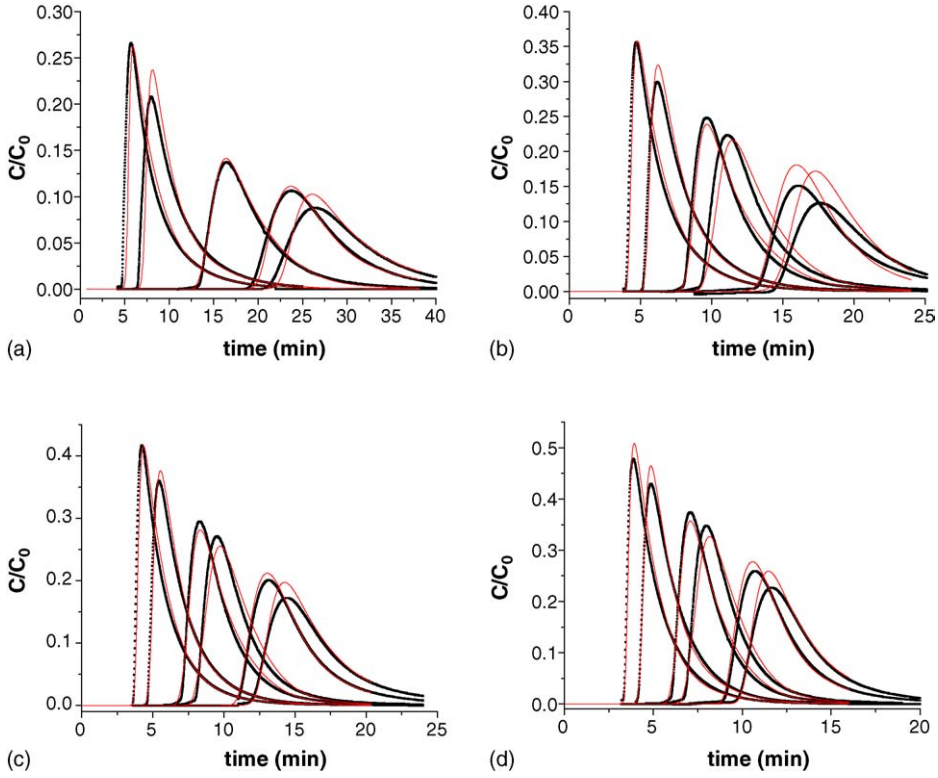

Fig. 8. Comparison between calculated and experimental peak profiles of: (a) Fmoc-L-Tyr at 298 K; (b) Fmoc-L-Tyr at 313 K; (c) Fmoc-L-Tyr at 323 K; (d) Fmoc-L-Tyr at 333 K. The y-axis is normalized by dividing the elute concentration with the injected concentration of the samples. The injection time was equal to 1 min. The following inlet concentrations were used: at 298 K 0.125, 0.245, 2.55, 24.8 and 49.6 mM; at 313 K 0.123, 0.245, 2.54, 5.089, 24.8, and 49.6 mM; at 323 K 0.126, 0.253, 2.54, 5.084, 25.0, and 49.9 mM; at 333 K 0.142, 0.285, 2.53, 5.062, 24.9, and 49.7 mM (peaks from right to left). The best values of parameters used to simulate these peak profiles are summarized in Table 7.

and the amount adsorbed, q, for Fmoc-L-Trp (closed circles), Fmoc-L-Tyr (closed squares), Fmoc-L-Ser (closed triangle-ups), and Fmoc-L-Phe (open triangle-downs). The decrease of Q_{st} (the amount of energy released during adsorption) with increasing q can be observed for all the L-enantiomers studied, illustrating the surface energetic heterogeneity for the L-enantiomers on the MIP. The relationship between Q_{st} and q was correlated using the following empirical equation: [5]

$$\frac{-Q_{st}}{R} = p_1 + p_2 \times \exp(-p_3 \times q) + p_4 \times \exp(-p_5 \times q) \quad (10)$$

The solid lines in Fig. 6 represent the best values of the parameters (i.e., p_1, p_2, p_3, and p_4 in Eq. (9)) which are summarized in Table 6. Combination of Eqs. (8) and (10) gives Eq. (11) to calculate the value of the surface diffusion coefficient that indirectly incorporates the contribution of surface heterogeneity.

$$D_S(Q_{st}) = D_{S0} \exp\left(\frac{-\alpha}{T}(p_1 + p_2 \times \exp(-p_3 \times q) + p_4 \times \exp(-p_5 \times q))\right) \quad (11)$$

This heterogeneous surface diffusion coefficient was used to calculate the band profiles of the L-enantiomers on the MIP at each temperature by optimizing the parameters D_{S0} and α for best agreement between the experimental and the calculated band profiles. The optimized values of D_{S0} and α for the L-enantiomers are summarized in Table 7. Figs. 7–10 compare experimental and calculated band profiles for Fmoc-L-Trp, Fmoc-L-Tyr, Fmoc-L-Ser, and Fmoc-L-Phe, respectively, on the MIP at each temperature. There is a very a good agreement between the two sets of band profiles for each substrate.

Fig. 11 shows the plots of the surface diffusivities versus q for Fmoc-L-Trp (Fig. 11(a)), Fmoc-L-Tyr (Fig. 11(b)), Fmoc-L-Ser (Fig. 11(c)), and Fmoc-L-Phe (Fig. 11(d))on the MIP. The values of the surface diffusivities derived from Eq. (11) at different values of the amount adsorbed (q) for each substrate are also summarized in Table 5. These values illustrate the dependency of the surface diffusivities on the amount adsorbed and show that these diffusivities increase with increasing temperature. The surface diffusivities of the L-enantiomers are between 5×1^{-7} and 5×10^{-6}, values comparable with the surface diffusivities of small molecules reported on a reversed phase stationary phase [22] and to those measured for the

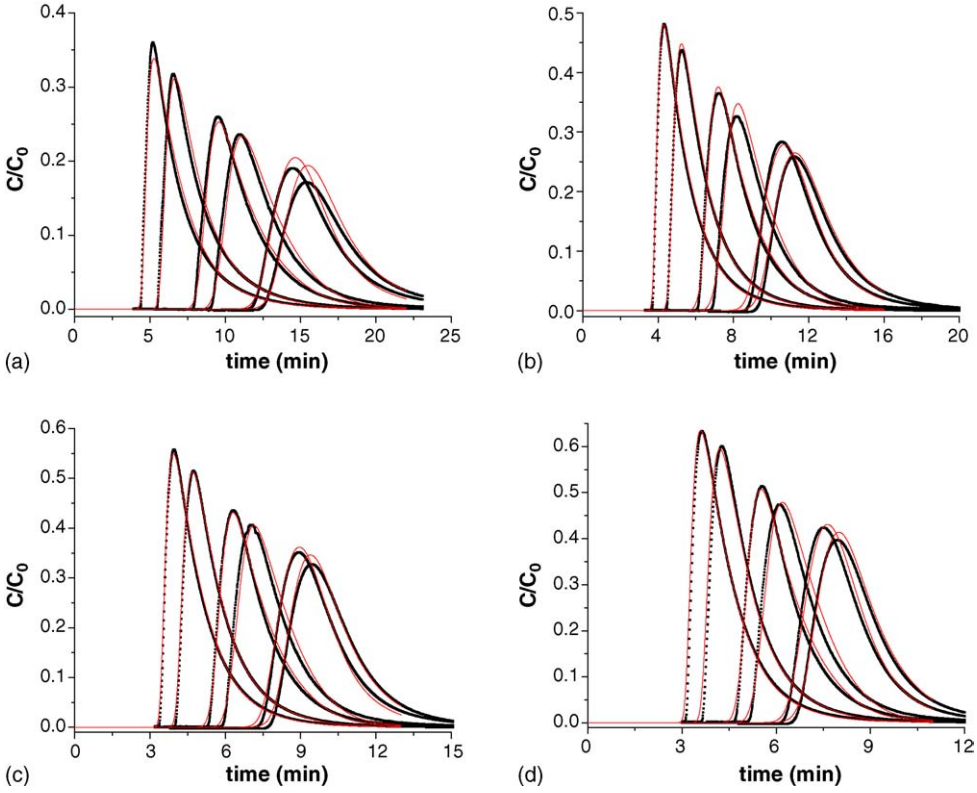

Fig. 9. Comparison between calculated and experimental peak profiles of: (a) Fmoc-L-Ser at 298 K; (b) Fmoc-L-Ser at 313 K; (c) Fmoc-L-Ser at 323 K; (d) Fmoc-L-Ser at 333 K. The y-axis is normalized by dividing the elute concentration with the injected concentration of the samples. The injection time was equal to 1 min. The following inlet concentrations were used: at 298 K 0.170, 0.339, 3.068, 6.14, 27.6 and 55.1 mM; at 313 K 0.1604, 0.3208, 3.12, 6.25, 27.5, and 55.1 mM; at 323 K 0.176, 0.351, 3.099, 6.20, 27.5, and 55.03 mM; at 333 K 0.177, 0.354, 3.066, 6.03, 27.5, and 55.1 mM (peaks from right to left). The best values of parameters used to simulate these peak profiles are summarized in Table 7.

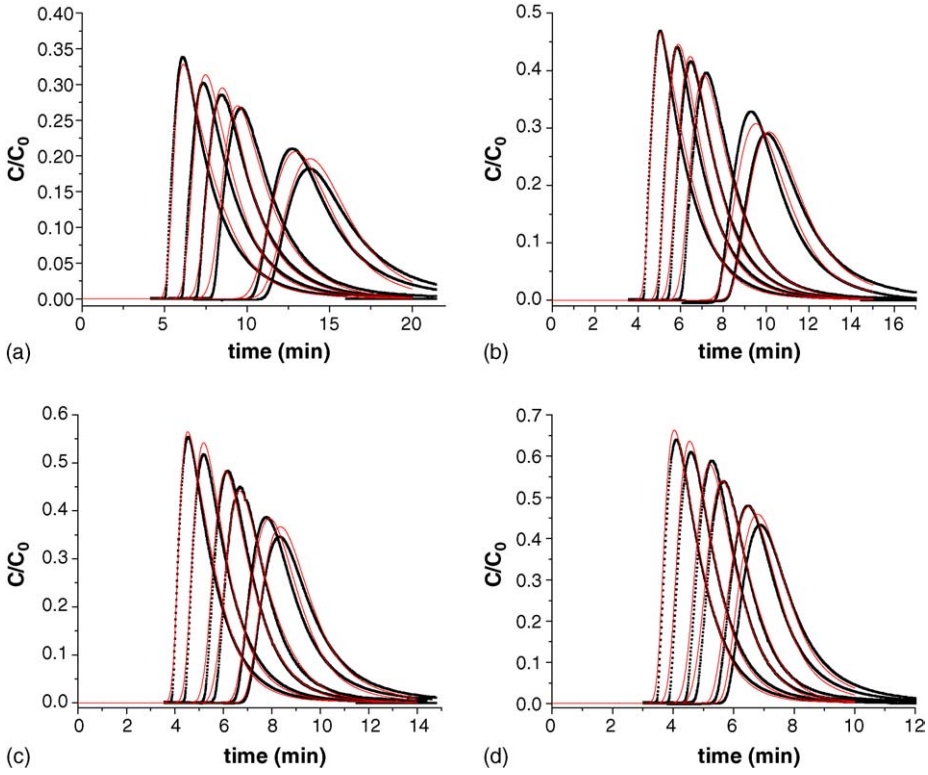

Fig. 10. Comparison between calculated and experimental peak profiles of: (a) Fmoc-L-Phe at 298 K; (b) Fmoc-L-Phe at 313 K; (c) Fmoc-L-Phe at 323 K; (d) Fmoc-L-Phe at 333 K. The *y*-axis is normalized by dividing the elute concentration with the injected concentration of the samples. The injection time was equal to 1 min. The following inlet concentrations were used: at 298 K 0.132, 0.274, 2.70, 5.25, 10.33 and 20.67 mM; at 313 K 0.133, 0.265, 2.53, 5.055, 9.013, and 18.03 mM; at 323 K 0.141, 0.283, 1.27, 2.54, 8.702, and 17.4 mM; at 333 K 0.138, 0.275, 1.38, 2.77, 8.72, and 17.4 mM (peaks from right to left). The best values of parameters used to simulate these peak profiles are summarized in Table 7.

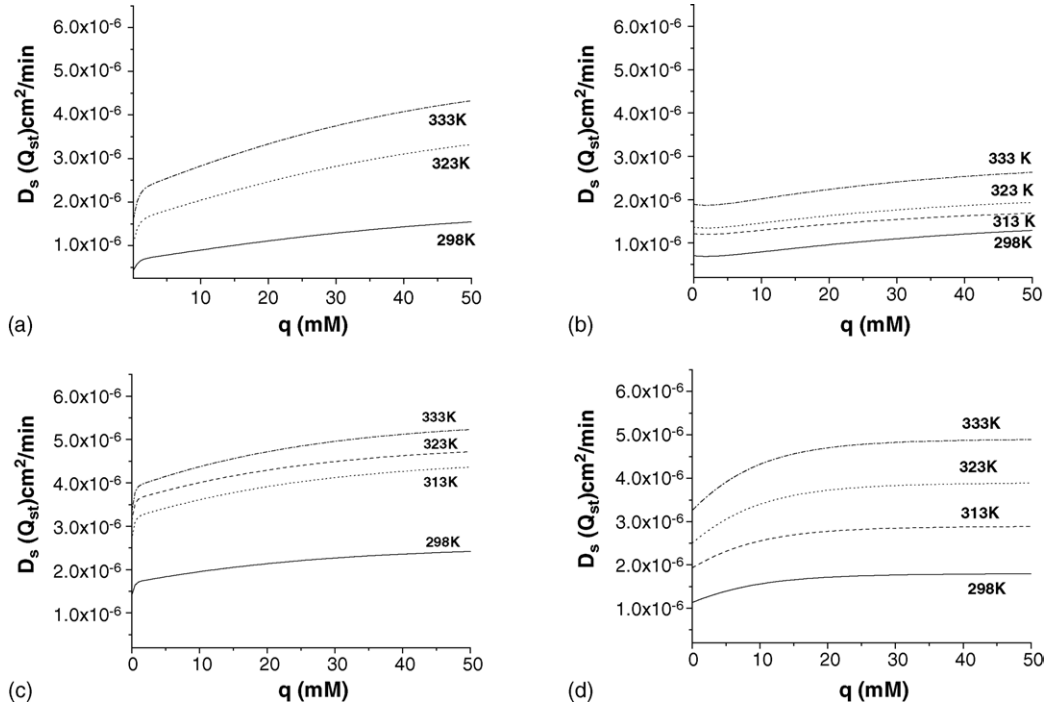

Fig. 11. The dependency of surface diffusion coefficients (D_s) on the amount adsorbed (q) for: (a) Fmoc-L-Trp; (b) Fmoc-L-Tyr; (c) Fmoc-L-Ser; (d) Fmoc-L-Phe.

phenylalanine enantiomers on a L-phenylalanine MIP [21]. At low amounts adsorbed (i.e., $q < 0.5$) and at all temperatures, the surface diffusivities of the L-enantiomers ($D_s(Q_{st})$) decrease in the following order:

Fmoc-L-Phe > Fmoc-L-Ser > Fmoc-L-Tyr > Fmoc-L-Trp

These results show that the surface diffusivities decrease with increasing affinity of the substrate for the highest energy sites (see Tables 1 and 5) at low amounts adsorbed. When the amount adsorbed becomes higher than 0.5 mM (Table 5), these surface diffusivities decrease in the following order:

Fmoc-L-Phe > Fmoc-L-Ser > Fmoc-L-Trp > Fmoc-L-Tyr.

Thus, at high amounts adsorbed, the surface diffusivities decrease with increasing overall affinity of the substrates for the MIP.

5. Conclusion

We measured by FA the equilibrium isotherms of several compounds that are structurally analogue to the template (Fmoc-L-Trp) of a MIP and have the same stereochemistry. These isotherms are correctly modeled by the tri-Langmuir isotherm. Comparison of the isotherm parameters for each L-enantiomer on the MIP show that the affinity of the L-enantiomers and the selectivity of the highest energy types of sites against the template on the MIP increases with increasing number of –OH groups on the substrates. Thermodynamic functions derived from the van't Hoff plot show that enthalpy is the driving force for the affinity of the L-enantiomers on the MIP.

The intraparticle mass transfer parameters of the L-enantiomers on the MIP were estimated by calculating the experimental band profiles using the POR model for chromatography with the tri-Langmuir isotherm model. The dominant mass transfer mechanism of the L-enantiomers on the MIP is surface diffusion. The dependency of surface diffusivities on the sample concentration was modeled by incorporating surface heterogeneity into the surface diffusion coefficients, using the empirical relationship between the isosteric heat of adsorption and the amount adsorbed. These heterogeneous surface diffusivities decrease with increasing affinity of the L-enantiomers on the MIP.

Acknowledgments

This work was supported in part by grant CHE-02-44693 of the National Science Foundation, by grant DE-FG05-88-ER-13869 of the US Department of Energy, and by the cooperative agreement between the University of Tennessee and the Oak Ridge National Laboratory.

References

[1] B. Sellergren (Ed.), Molecularly Imprinted Polymers. Man-made Mimics of Antibodies and Their Applications in Analytical Chemistry, Elsevier, Amsterdam, The Netherlands, 2001.
[2] H. Kim, G. Guiochon, Anal. Chem., in press.
[3] H. Kim, K. Kaczmarski, G. Guiochon, Chem. Eng. Sci., in press.
[4] H. Kim, G. Guiochon, Anal. Chem. 77 (2005) 1708.
[5] H. Kim, K. Kaczmarski, G. Guiochon, Chem. Eng. Sci 60 (2005) 5425.
[6] K. Kaczmarski, D. Antos, H. Sajonz, P. Sajonz, G. Guiochon, J. Chromatogr. A 925 (2001) 1.
[7] D. Antos, K. Kaczmarski, W. Piatkowski, A. Seidel-Morgenstern, J. Chromatogr. A 1006 (2003) 61.
[8] G. Guiochon, S.G. Shirazi, A.M. Katti, Fundamentals of Preparative and Nonlinear Chromatography, Academic Press, Boston, MA, 1994.
[9] P. Sajonz, G. Zhong, G. Guiochon, J. Chromatogr. A 731 (1996) 1.
[10] log P_{ow} (octanol–water partition coefficient) was calculated using Kow Win program available for free of charge at http://esc.syrres.com/interkow/physdemo.htm.
[11] H. Kim, G. Guiochon, Anal. Chem. 77 (2005) 93.
[12] M. Lehmann, M. Dettling, H. Brunner, G.E.M. Tovar, J. Chromatogr. B 808 (2004) 43.
[13] H. Kim, K. Kaczmarski, G. Guiochon, J. Chromatogr. A, submitted for publication.
[14] T. Fornstedt, P. Sajonz, G. Guiochon, J. Am. Chem. Soc. 119 (1997) 1254.
[15] S. Jacobson, S. Golshan-Shirazi, G. Guiochon, J. Chromatogr. 522 (1990) 22.
[16] V.P. Joshi, M.G. Kulkarni, R.A. Mashelkar, Chem. Eng. Sci. 55 (2000) 1509.
[17] B. Sellergren, K.J. Shea, J. Chromatogr. A 690 (1995) 29.
[18] W.-Y. Chen, C.-S. Chen, F.-Y. Lin, J. Chromatogr. A 923 (2001) 1.
[19] Y. Lu, C. Li, H. Zhang, X. Liu, Anal. Chim. Acta 489 (2003) 33.
[20] P. Sajonz, M. Kele, G. Zhong, B. Sellergren, G. Guiochon, J. Chromatogr. A 810 (1998) 1.
[21] K. Miyabe, G. Guiochon, Biotechnol. Prog. 16 (2000) 617.
[22] K. Miyabe, G. Guiochon, Anal. Chem. 73 (2001) 3096.